THE JOURNAL OF PHYSICAL CHEMISTRY C

Article

pubs.acs.org/JPCC

Some Quinoxalin-6-yl Derivatives as Corrosion Inhibitors for Mild Steel in Hydrochloric Acid: Experimental and Theoretical Studies

Lukman O. Olasunkanmi,[†,‡,§] Ime B. Obot,[∥] Mwadham M. Kabanda,[†,‡] and Eno E. Ebenso*[,†,‡]

[†]Department of Chemistry, School of Mathematical and Physical Sciences, Faculty of Agriculture, Science and Technology, North-West University (Mafikeng Campus) Private Bag X2046, Mmabatho 2735, South Africa

[‡]Material Science Innovation and Modelling (MaSIM) Research Focus Area, Faculty of Agriculture, Science and Technology, North-West University (Mafikeng Campus) Private Bag X2046, Mmabatho 2735, South Africa

[§]Department of Chemistry, Faculty of Science, Obafemi Awolowo University, Ile-Ife 220005, Nigeria

[∥]Centre of Research Excellence in Corrosion, Research Institute, King Fahd University of Petroleum and Minerals, Dhahran 31261, Kingdom of Saudi Arabia

ABSTRACT: The inhibition of mild steel corrosion in 1 M HCl by some quinoxalin-6-yl derivatives namely 1-[3-phenyl-5-quinoxalin-6-yl-4,5-dihydropyrazol-1-yl]butan-1-one (PQDPB), 1-(3-phenyl-5-(quinoxalin-6-yl)-4,5-dihydro-1*H*-pyrazol-1-yl)propan-1-one (PQDPP), and 2-phenyl-1-[3-phenyl-5-(quinoxalin-6-yl)-4,5-dihydropyrazol-1-yl]-ethanone (PPQDPE) has been investigated using electrochemical studies and quantum chemical calculations. The results showed that PQDPP is the best corrosion inhibitor among the three compounds studied and the inhibition efficiency increases with increase in concentration for all the inhibitors. The adsorption of inhibitor molecules on mild steel surface was found to be spontaneous and obeyed the Frumkin adsorption isotherm. Scanning electron microscopy (SEM) images confirmed the formation of protective films of the inhibitors on mild steel surface. Quantum chemical calculations showed that the inhibitors have the tendency to be protonated in the acid and the results agree with experimental observations. Monte Carlo simulations were applied to search for the most stable configuration and adsorption energy for the interaction of inhibitors on Fe(110)/100 H_2O interface. The results of the Monte Carlo simulations accord with the experimentally determined inhibition efficiencies. Different carbonyl substituents on the common nucleus of the three compounds obviously contributed to the difference in inhibition efficiency.

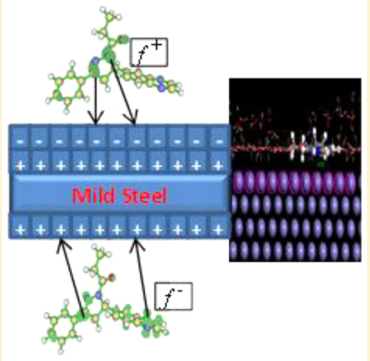

1. INTRODUCTION

Corrosion of metals is of major economic and safety concern to many industries including construction and oil-refining industries.[1,2] Mild steel is a widely used metal in most industries due to its relatively low cost and good mechanical strength.[3,4] The use of corrosion inhibitors has been a popular method of protecting the surface of active metals against corrosion in various media.[5−7] It is the simplest method of reducing corrosion rate until date, and it is relatively cheap.[2,7,8] Nitrogen-, oxygen-, and sulfur-containing organic compounds, especially those with π-electron systems are commonly considered as corrosion inhibitors, and many of them have been reported to have appreciable inhibition efficiencies.[8−10]

Quinoxaline derivatives are popular nitrogen−heterocyclic compounds that have attracted much attention in the past few years. These compounds are easy to synthesize, are environmentally friendly, and exhibit wide biological and photochemical activities.[11−14] It is against this backdrop that different quinoxaline derivatives are continuously being synthesized and studied for diverse potential applications. Many quinoxaline derivatives have been reported as efficient inhibitors of metal corrosion in acidic medium in the past few years.[15−26] The design of new corrosion inhibitors and the study of their inhibition properties are gaining increasing attention from materials scientists and engineers.

Electrochemical techniques such as potentiodynamic polarization and electrochemical impedance spectroscopy have been successfully utilized to study electrochemical corrosion, and determine inhibition properties of corrosion inhibitors. But theoretical approaches are often used to make in-depth explanations of the experimental results. In this regard, quantum chemical calculations are usually employed to correlate molecular properties of inhibitor molecules with inhibition efficiencies.[8,12,16,21,24] In addition, adequate description of the interactions between the inhibitor molecules and the metal surfaces is important in designing and investigating new corrosion inhibitors and molecular dynamic simulation has proven to be efficient tool in examining these interactions.[24,27−32]

The objective of the present work is to examine the anticorrosive properties of three quinoxalin-6-yl derivatives namely 1-[3-phenyl-5-quinoxalin-6-yl-4,5-dihydropyrazol-1-yl]-

Received: April 5, 2015
Revised: June 25, 2015
Published: June 26, 2015

DOI: 10.1021/acs.jpcc.5b03285
J. Phys. Chem. C 2015, 119, 16004−16019

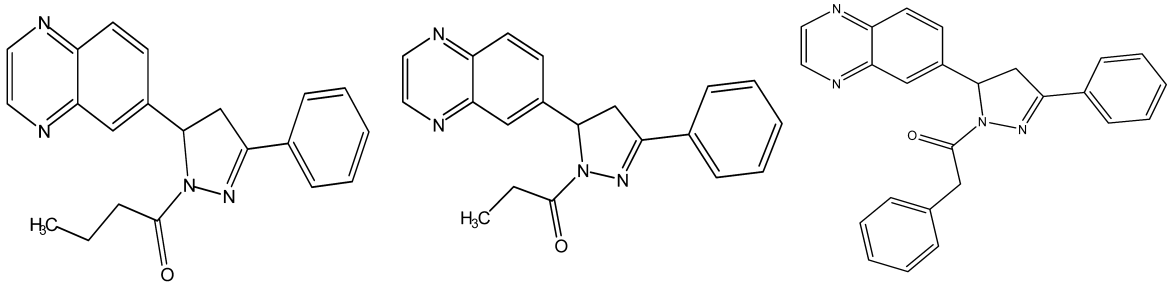

1-[3-phenyl-5-quinoxalin-6-yl-4,5-dihydropyrazol-1-yl]butan-1-one (PQDPB)

1-(3-phenyl-5-(quinoxalin-6-yl)-4,5-dihydro-1H-pyrazol-1-yl)propan-1-one (PQDPP)

2-phenyl-1-[3-phenyl-5-(quinoxalin-6-yl)-4,5-dihydropyrazol-1-yl]ethanone (PPQDPE)

Figure 1. Structures of PQDPB, PQDPP, and PPQDPE.

butan-1-one (PQDPB), 1-(3-phenyl-5-(quinoxalin-6-yl)-4,5-dihydro-1*H*-pyrazol-1-yl)propan-1-one (PQDPP) and 2-phenyl-1-[3-phenyl-5-(quinoxalin-6-yl)-4,5-dihydropyrazol-1-yl]-ethanone (PPQDPE) on the corrosion of mild steel in hydrochloric acid medium. Potentiodynamic polarization and electrochemical impedance spectroscopic techniques were used for electrochemical studies, while ab initio HF/6-31G(d) and DFT B3LYP/6-31G(d) methods were used for the quantum chemical calculations. The possibility of protonation of potential basic sites of inhibitor molecule in acidic environment is not usually taken into consideration when correlating quantum molecular parameters with experimental inhibition efficiency. However, since there have been few reports that inhibitor molecules with donor sites have the tendency of being protonated in acidic environment and the inhibition properties sometimes depend on the quantum chemical properties of the protonated species,[10,33] a detailed quantum chemical study of singly protonated forms of the studied compounds was carried out at all possible sites of protonation in addition to the study on the neutral molecules. Monte Carlo simulations were applied to search for the most stable configuration and adsorption energy for the interaction of inhibitors on Fe (110)/100 H_2O interface. The chemical structures of the compounds studied are presented in Figure 1. To the best of our knowledge, this is the first time these set of quinoxaline derivatives are being investigated as corrosion inhibitors. The set of quinoxaline derivatives studied in this work has 4,5-dihydro-1*H*-pyrazol-5-yl group as a substituent on the quinoxaline ring. The 4,5-dihydro-1*H*-pyrazol-5-yl substituent is also substituted by a carbonyl and phenyl groups on positions 1 and 3 respectively. The set of compounds considered in this work have common nucleus, and differ only in the chain of the carbonyl group attached to the first nitrogen atom of the dihydropyrazole ring, i.e., butyl (in PQDPB), propyl (in PQDPP), and phenylethyl (in PPQDPE). Therefore, electronic and steric hindrance effects of the substituent carbonyl functional groups on the corrosion inhibition efficiencies will be investigated. The presence of multiple π-electron rings and/or units and heteroatoms portrays these compounds as prospective efficient corrosion inhibitors.

2. EXPERIMENTAL DETAILS

2.1. Materials and Sample Preparation. All reagents and solvents used in the experiment were of analytical grade and used without further purification. The mild steel used in this study has the chemical composition (in wt %) of C = 0.17, M_n = 0.46, Si = 0.26, S = 0.017, and P = 0.019, and balance Fe. For the purpose of electrochemical studies, mild steel coupon was cut into 1 cm × 1 cm and embedded in a Teflon holder using epoxy resin, exposing a surface area of 1 cm^2. Mild steel surface was mechanically abraded on Struers MD Piano 220 (size: 200 dia) mounted on Struers LaboPol-1 machine to remove traces of epoxy resin from the surface. The surface was then polished with SiC paper of graded grit sizes ranging from 600 to 1200 to achieve a mirror-shining surface. Mild steel surface was then washed with water, degreased in acetone and then washed with water again, before finally dried with clean white towel paper.

The aggressive solution of 1 M HCl was prepared by diluting the analytical grade 32% (Promark Chemicals) with distilled water. The inhibitors were purchased from Vitas-M Laboratory, Ltd., Moscow. The concentrations of inhibitors used are 10, 20, 40, and 60 ppm.

2.2. Electrochemical Measurements. All electrochemical measurements were carried out on the Autolab PGSTAT 302N from Metrohm equipped with a three-electrode system and controlled by Nova 1.10.1.9 software. Ag/AgCl with 3 M KCl was used as the reference electrode, while platinum rod was used as the counter electrode. Mild steel with a freshly prepared shining surface of 1 cm^2 surface area was used as the working electrode. A period of 30 min was allowed for the system to reach the steady open circuit potential (OCP) before each electrochemical measurement. Potentiodynamic polarization studies were performed after 30 min of mild steel immersion in the aggressive solutions by sweeping the potential between −100 and +100 mV vs the OCP, stepping at 1 mV/s scan rate. The electrochemical impedance spectroscopic (EIS) measurements were conducted at the OCP by analyzing the frequency response of the electrochemical system in the range of 100 kHz to 0.1 Hz at 5 mV amplitude. All electrochemical experiments were conducted under aerated unstirred conditions at 303 K. Corrosion inhibition efficiency (% IE_p) was calculated from polarization experiment as

$$\%\ IE_p = 100\left(\frac{i_{corr}^0 - i_{corr}}{i_{corr}^0}\right) \quad (1)$$

where i_{corr}^0 and i_{corr} are corrosion current densities in the absence and presence of inhibitors, respectively. For the impedance experiment, corrosion inhibition efficiency (% IE_I) was calculated from

DOI: 10.1021/acs.jpcc.5b03285
J. Phys. Chem. C 2015, 119, 16004−16019

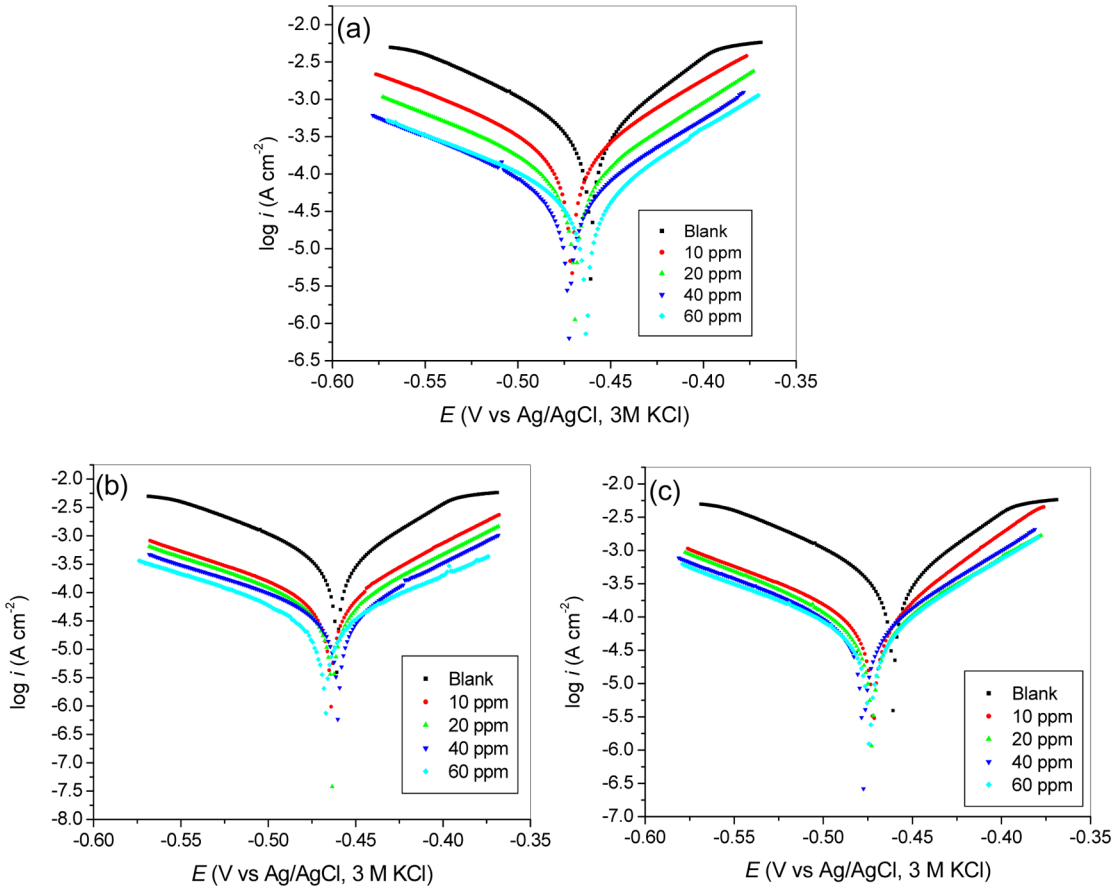

Figure 2. Polarization curves for mild steel in 1 M HCl without and with of various concentrations of (a) PQDPB, (b) PQDPP, and (c) PPQDPE.

$$\%\ \mathrm{IE}_I = 100\left(\frac{R_{ct} - R_{ct}^0}{R_{ct}}\right) \tag{2}$$

where R_{ct}^0 and R_{ct} are the charge transfer resistances without and with various concentrations of inhibitors, respectively.

2.3. Surface Analysis. Mild steel surface was prepared as discussed in section 2.1 above and then immersed in 1 M HCl without and with 60 ppm of each inhibitor for a period of 3 h. Thereafter, the specimens were retrieved from the solutions, rinsed with distilled water, degreased with acetone, wiped with a clean towel paper and finally air-dried. Scanning electron microscopic (SEM) analyses of the surfaces were carried out at an accelerating voltage of 15 kV on Microtrac Semtrac scanning electron microscope equipment.

2.4. Quantum Chemical Calculations. Geometry optimization and vibrational frequency calculations were carried out without symmetry constraint on both the neutral and protonated forms of the inhibitor molecules at HF/6-31G(d) (ab initio Hartree−Fock) and B3LYP/6-31G(d) (density functional theory (DFT)) levels of theory. All the calculated harmonic vibrational frequencies are real values indicating that the optimized structures correspond to energy minima. Calculations were carried out in the gas phase using Gaussian 09W version D.01 software.[34] Frontier molecular orbital (FMO) energy parameters including the highest occupied molecular orbital (HOMO) and lowest unoccupied molecular orbital (LUMO) energies were obtained for both the neutral and protonated forms of the inhibitor molecules. The HOMO energy (E_{HOMO}) and the LUMO energy (E_{LUMO}) are related to ionization potential (I) and electron affinity (A) as $I = -E_{\mathrm{HOMO}}$ and $A = -E_{\mathrm{LUMO}}$ respectively, in accordance with Koopman's theorem.[35] Absolute hardness, η, and absolute electronegativity, χ, of the inhibitors are calculated as

$$\eta = \frac{1}{2}(I - A) \tag{3}$$

$$\chi = \frac{1}{2}(I + A) \tag{4}$$

The fraction of electrons transferred (ΔN) from the inhibitor molecule (donor) to the metallic (Fe) atom (acceptor) was calculated using[36]

$$\Delta N = \frac{\chi_{Fe} - \chi_{inh}}{2(\eta_{Fe} + \eta_{inh})} \tag{5}$$

where χ and η denote the electronegativity and hardness, respectively. A value of 7 eV/mol was used for the χ_{Fe}, while η_{Fe} was equated to 0 eV/mol for bulk Fe atom in accordance to Pearson's electronegativity scale.[37]

Atom condensed Fukui functions for the electrophilic (f^+) and nucleophilic (f^-) active sites were calculated by applying the Mulliken population analysis (MPA) and the finite difference (FD) approximations approach introduced by Yang and Mortier,[38] and using the equations:

$$f_k^+ = \rho_{k(N+1)}(r) - \rho_{k(N)}(r) \tag{6}$$

$$f_k^- = \rho_{k(N)}(r) - \rho_{k(N-1)}(r) \tag{7}$$

where $\rho_{k(N+1)}$, $\rho_{k(N)}$, and $\rho_{k(N-1)}$ are the electron densities of the kth atom in a molecule with $N + 1$ electrons, N electrons, and

DOI: 10.1021/acs.jpcc.5b03285
J. Phys. Chem. C 2015, 119, 16004−16019

$N - 1$ electrons, respectively. Electron density values were approximated by Mulliken gross charges obtained from geometry optimizations. Fukui indices, f^+ and f^-, were calculated and visualized with Multiwfn software.[39,40]

2.5. Monte Carlo Simulations. Monte Carlo simulations using the adsorption locator code implemented in the Material Studio 7.0 software from Accelrys Inc. USA, was adopted to compute the adsorption energy of the interaction between the inhibitor molecules and clean iron surface in water. For the whole simulation procedure, the COMPASS force field was used to optimize the structures of all components of the system of interest. COMPASS (condensed-phase optimized molecular potentials for atomistic simulation studies) force field is an ab initio force field that enables accurate and simultaneous predictions of gas-phase properties (structural, conformational, vibrational, etc.) and condensed-phase (equation of state, cohesive energies, interaction energies, etc.) for a broad range of organic molecules and metals. Fe (110) crystal surface was selected for this simulation and to represent mild steel because it is the most stable surface. The simulation was carried out in a simulation box (29.78 Å × 29.78 Å × 58.10 Å) with periodic boundary conditions in order to simulate a representative part of an interface devoid of any arbitrary boundary effects. The Fe (110) plane was next enlarged to a (12 × 12) supercell. After that, a vacuum slab with 50 Å thickness was built above the Fe (110) plane. The three inhibitor molecules designated as PQDPB, PQDPP and PPQDPE along with 100 water molecules were used for the simulations in each case. The use of the water molecules is important since electrochemical corrosion inhibition process takes place in aqueous solution.

3. RESULTS AND DISCUSSION

3.1. Tafel Polarization Curves. Tafel polarization curves were obtained from potentiodynamic polarization measurements on mild steel in 1 M HCl without and with various concentrations of the inhibitors and the results are presented in Figure 2. The polarization curves in Figure 2 exhibit similar behavior for the three inhibitors as well as for 1 M HCl blank system. This suggests that the mechanism of inhibition is the same for all the inhibitors studied in this work, and that addition of inhibitors does not cause significant change in corrosion mechanism. More so, both anodic and cathodic reactions are inhibited. In other words, the inhibitors reduce the anodic dissolution of mild steel and also retard the rate of cathodic H^+ ions reduction. The results obtained for the electrochemical kinetic parameters including the corrosion potential (E_{corr}), corrosion current density (i_{corr}), anodic and cathodic Tafel slopes (β_a and β_c respectively) are listed in Table 1. The shift in E_{corr} at various concentrations of the inhibitors does not follow a definite pattern. However, the maximum value of the difference in E_{corr} between the blank and the inhibitor-containing systems was 16.78 mV (i.e., E_{corr} for 40 ppm PPQDPE vs blank), which suggests that the studied compounds are mixed-type inhibitors. The small shifts in E_{corr} lie toward more negative potentials associated with cathodic branch of electrochemical corrosion. This implies that the mixed-type inhibition effects of the studied compounds are slightly more pronounced on reduction of H^+ ions.[41] The corrosion current density, i_{corr} decreases with increase in concentration of the inhibitors leading to increase in inhibition efficiency (% IE_P). The order of inhibition efficiency of the three inhibitors at 60 ppm (maximum concentration studied) is PQDPP > PQDPB > PPQDPE. However, the % IE_P of PPQDPE is greater than that of PQDPB at 10 and 20 ppm (lower concentrations). The enhanced inhibition potency of PQDPB at higher concentrations (40 and 60 ppm) was attributed to the possibility of multiple protonation of available basic sites on the compound in the acid. A more detailed theoretical explanation is provided for this possibility in the later sections (*vide infra*, quantum chemical calculations).

Table 1. Electrochemical Potentiodynamic Polarization Parameters and Percentage Inhibition Efficiency for the Corrosion of Mild Steel in 1 M HCl without and with Inhibitors

compound	concn (ppm)	$-E_{corr}$ (mV)	i_{corr} (μA/cm^2)	β_a (mV/dec)	β_c (mV/dec)	% IE_P
blank	–	460.60	420.41	89.34	65.27	–
PQDPB	10	471.17	204.04	98.82	74.51	51.47
	20	469.37	95.54	94.30	70.91	77.28
	40	472.61	58.86	102.28	75.33	86.00
	60	463.02	51.34	106.11	69.16	87.79
PQDPP	10	464.22	79.32	102.92	65.56	81.13
	20	463.42	60.71	102.34	70.44	85.56
	40	459.97	48.85	112.90	70.42	88.38
	60	467.36	39.51	110.61	94.39	90.60
PPQDPE	10	471.86	88.78	95.49	55.10	78.88
	20	472.59	77.22	96.20	74.00	81.63
	40	477.38	68.50	96.53	67.12	83.71
	60	474.03	59.22	103.56	67.08	85.91

3.2. Electrochemical Impedance Spectroscopy. Nyquist and Bode plots were obtained for mild steel in 1 M HCl without and with various concentrations of the three inhibitors and the results are shown in Figures 3 and 4 respectively. The Nyquist plots show a single depressed capacitive arc over the frequency range studied. The Nyquist plots exhibit oval semicircular shapes, which are commonly observed for solid electrodes as a result of frequency dispersion of interfacial impedance. This feature is usually attributed to different factors such as surface roughness, impurities, discontinuity in the electrode, adsorption of inhibitor and inhomogeneity of the electrode surface.[42] Similarity in the shapes of these plots for the uninhibited and inhibited systems implies that the inhibitors reduce the corrosion rate without changing the corrosion mechanism.[42,43] The results also reveal that mild steel dissolution in the studied aggressive media is controlled by a single charge transfer process.[41,44] The Nyquist plots exhibit large capacitive loops at high frequencies and small inductive loops at low frequencies. The capacitive loop at high frequency is usually associated with charge transfer process and electrical double layer.[9,45−47] The inductive loop at low frequency region may be attributed to relaxation process as a result of adsorption of species like Cl^-, H^+, or protonated inhibitor ($inhH^+$) ions on the electrode surface.[44,47,48] It might also be attributed to redissolution of the passivated surface at low frequencies.[46−48] As shown in Figure 3, the diameter of the capacitive loop in the presence of inhibitor is larger than that in the uninhibited system and increases with increase in concentration of the inhibitors. This implies that the inhibitors protect the steel surface against acid attack and the protection is enhanced at higher concentration of inhibitors.

The high frequency intercept with the real axis on the Nyquist plots corresponds to the solution resistance (R_s), while the low frequency intercept with the real axis is ascribed to the sum of the solution resistance (R_s) and the charge transfer

DOI: 10.1021/acs.jpcc.5b03285
J. Phys. Chem. C 2015, 119, 16004−16019

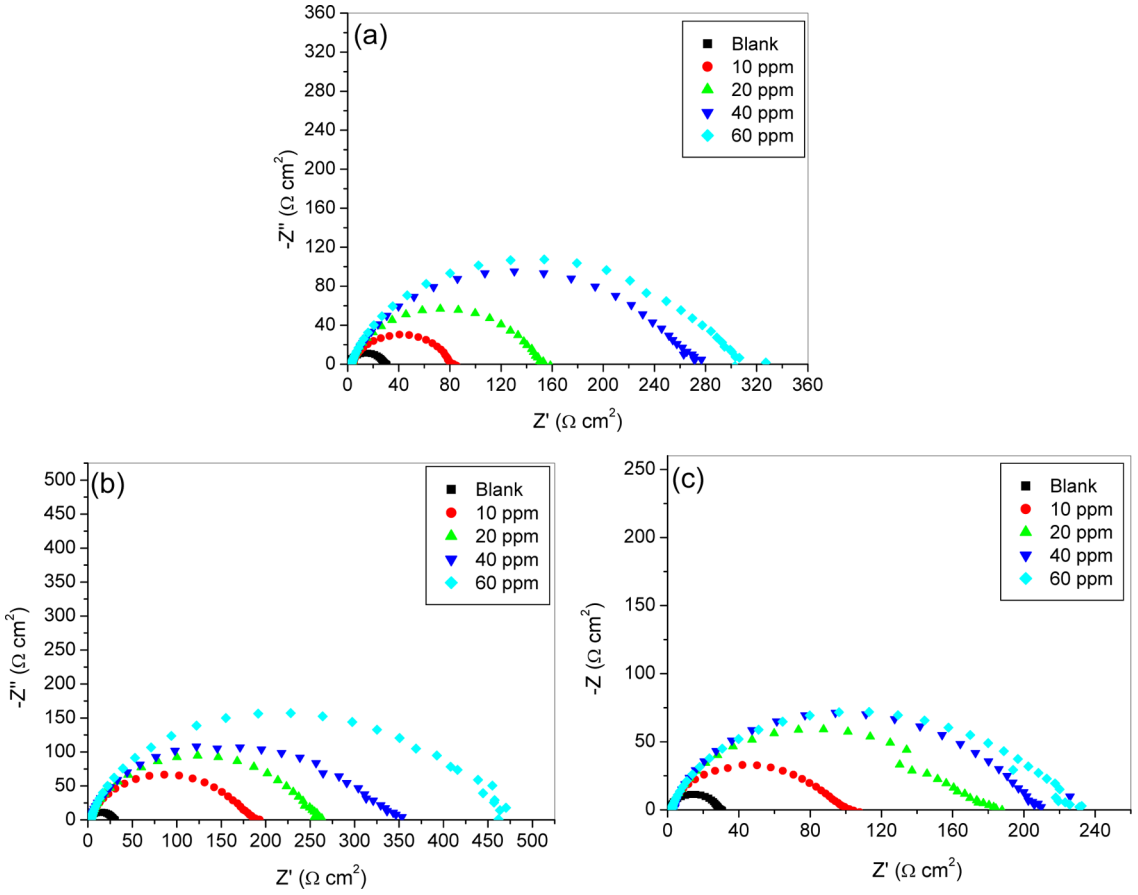

Figure 3. Nyquist plots for mild steel in 1 M HCl without and with various concentrations of (a) PQDPB, (b) PQDPP, and (c) PPQDPE.

resistance (R_{ct}), such that $R_{ct} = Z'(\text{low freq}) - Z'(\text{high freq})$. Electrochemical impedance kinetic parameters were obtained by fitting the impedance spectra to the equivalent circuit model $R_s(Q_{dl}R_{ct})$, in which the solution resistance is shorted by a constant phase element (CPE) that is in parallel connection to the charge transfer resistance. The impedance (Z) of the CPE is defined as[49]

$$Z_{CPE} = Y_o^{-1}(j\omega)^{-n} \tag{8}$$

where Y_o is the CPE constant (in $\mu Ss^n cm^{-2}$), $j^2 = -1$ is the imaginary number, ω is the angular frequency (in $rads^{-1}$), and n is a CPE exponent, which can be used as a gauge of the heterogeneity or roughness of the surface.[50] The results of the fitting and simulation analyses of the EIS profiles are listed in Table 2. Solution resistance is a significant factor in the impedance of an electrochemical cell and it is the characteristic of the cell. The values obtained for R_s (Table 2) are generally higher for the inhibitors-containing electrochemical systems compared to the blank acid solution. This implies that the solution conductivity is reduced by the addition of the inhibitors. The R_s values do not show any regular pattern with increasing concentration of the inhibitors because the geometry of the area through which the current is transported in the systems may not be the same. The values of Y_o are lower in the presence of inhibitors compared to that of uninhibited blank system. This can be attributed to gradual displacement of water molecules by inhibitor molecules at metal/solution interface leading to formation of protective layer on the steel surface.[9,51,52] The values of the CPE exponent, n are reduced by the addition of inhibitors. This suggests that the surface inhomogeneity of the electrode increases in the presence of the inhibitors, which again is an indication of adsorption of the inhibitors on the steel surface.[9] The increased values of R_{ct} with increasing concentration of the inhibitors can be attributed to increase in insulated adsorbed layer at the metal/solution interface. The values of % IE_I (inhibition efficiency from impedance experiment) also increase with increase in concentration of inhibitors, with PQDPP having a maximum value of 93.65% at 60 ppm. The mean difference between the values of % IE_I and % IE_P (inhibition efficiencies from impedance and polarization studies respectively) is between 3.0 and 5.4% and the trend of % IE_I for the three inhibitors is the same as that observed from the polarization studies (see Figure 5).

3.3. Adsorption Isotherms. Adsorption behavior of an inhibitor on a metal surface can be explained by fitting the experimental data into suitable adsorption isotherm(s). Inhibitor molecules tend to compete with water molecules for adsorption sites on metal surface. The displacement of water molecules by the inhibitor molecules follows the equation:[50]

$$Inh_{(sol)} + xH_2O_{(ads)} \leftrightarrow Inh_{(ads)} + xH_2O_{(sol)} \tag{9}$$

where x is the number of water molecules displaced by one molecule of organic inhibitor. The experimental data were subjected to various adsorption isotherms including Langmuir, Frumkin, and Temkin, but both Langmuir and Frumkin isotherms gave better fits with $R^2 > 0.9$. However, thermodynamic and interaction parameters were calculated for the studied molecules based on the slopes and intercepts

DOI: 10.1021/acs.jpcc.5b03285
J. Phys. Chem. C 2015, 119, 16004−16019

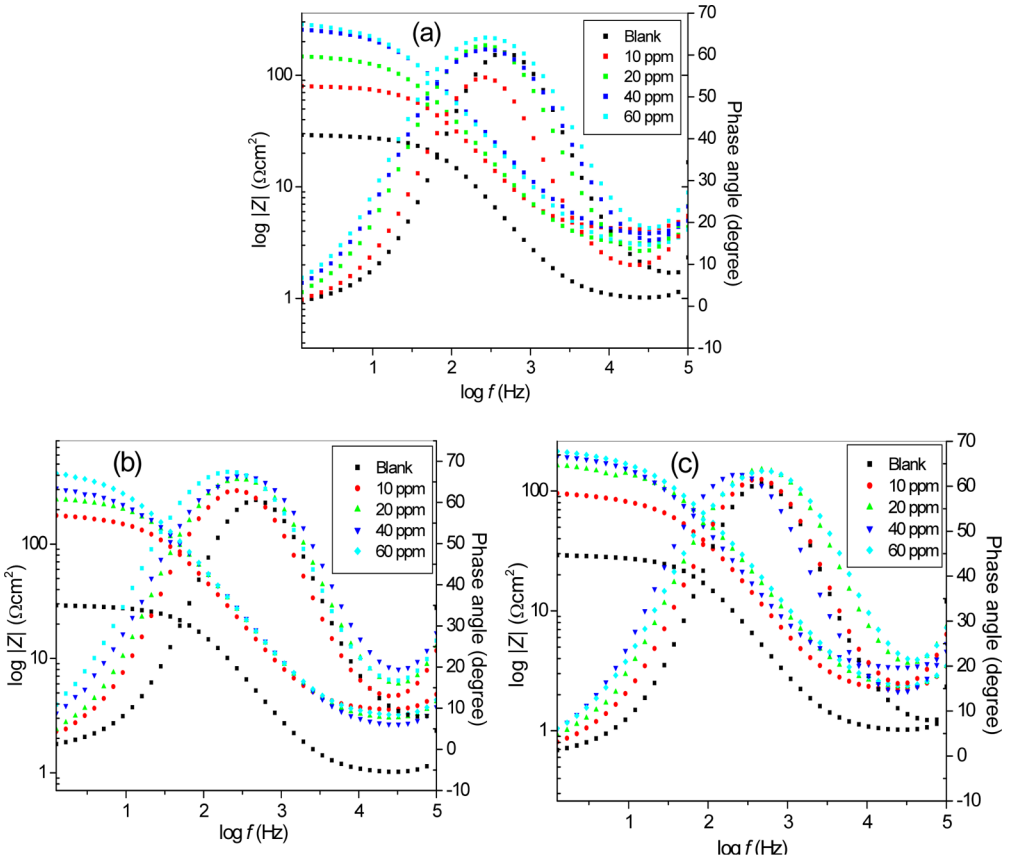

Figure 4. Bode plots for mild steel in 1 M HCl without and with various concentrations of (a) PQDPB, (b) PQDPP, and (c) PPQDPE.

Table 2. EIS Kinetic Parameters and Percentage Inhibition Efficiency for the Corrosion of Mild Steel in 1 M HCl without and with Inhibitors

compound	concn (ppm)	R_s (Ω cm^2)	R_{ct} (Ω cm^2)	Y_o (μS s^n cm^{-2})	n	% IE_I
blank	–	1.01	28.20	157	0.893	–
PQDPB	10	4.14	77.20	98.30	0.867	63.47
	20	3.02	148.00	88.90	0.856	80.90
	40	2.83	263.00	76.20	0.842	89.28
	60	2.76	297.00	77.40	0.820	90.50
PQDPP	10	3.46	178.00	75.40	0.857	84.16
	20	2.86	250.00	66.40	0.851	88.72
	40	2.37	321.00	81.30	0.822	91.21
	60	3.00	444.00	75.80	0.834	93.65
PPQDPE	10	2.09	93.80	106.00	0.845	69.94
	20	2.08	166.00	84.20	0.835	83.01
	40	3.24	199.00	97.10	0.822	85.83
	60	2.05	215.00	87.30	0.803	86.88

obtained from the Frumkin adsorption isotherms. The preference for the Frumkin adsorption isotherm is partly due its more realistic consideration of the real properties of a two-dimensional surface state of the adsorption layer, which in a way takes the surface molecular area of the adsorbed molecules and their intermolecular interactions into consideration.[53] The data from the EIS measurements were subjected to the linearized Frumkin adsorption isotherm equation of the form

$$\ln\left[\frac{\theta}{C(1-\theta)}\right] = \ln K_{ads} + 2a\theta \qquad (10)$$

where θ is the degree of surface coverage (θ = % IE_I/100), C is the concentration of the inhibitor, K_{ads} is the equilibrium constant of the adsorption process, and a is the interaction parameter, which predicts the nature of interaction (attraction, repulsion or none) that exists between the adsorbed species. As reported in literature,[54] a value of $a > 0$ implies an attraction between the adsorbed species, a value of $a < 0$ is an indication of repulsion between the adsorbed species, while a value of a = 0 implies lack of interaction between the adsorbed species. The Frumkin adsorption plots for the studied compounds are shown in Figure 6. The plots in Figure 6 contain seven-data points due to the inclusion of surface coverage (θ) at 5, 80, and 100 ppm (i.e., additional data points were put above and below the reported values in Table 2 in order to eliminate or reduce possible bias of the linearized form of the adsorption isotherm

DOI: 10.1021/acs.jpcc.5b03285
J. Phys. Chem. C 2015, 119, 16004−16019

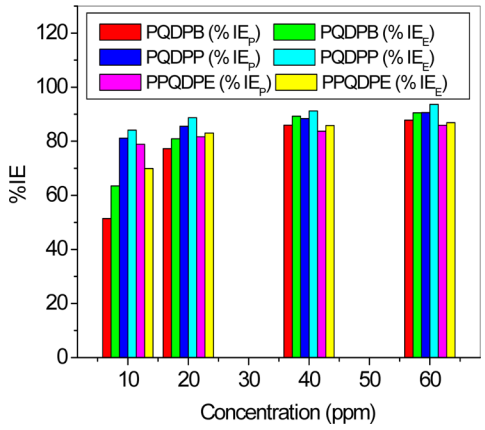

Figure 5. Variation of % IE with concentration of inhibitors for both polarization and impedance experiments.

which is usually more pronounced in the short concentration range). The $\%IE_I$ values for PQDPB, PQDPP and PPQDPE respectively are 31.05, 71.80, and 55.24% at 5 ppm; 91.94, 93.84, and 87.00 at 80 ppm; and 92.21, 94.97, and 90.51% at 100 ppm.

The change in free energy of adsorption (ΔG_{ads}) was calculated from the relation:[55]

$$\Delta G_{ads} = -RT \ln(55.5K_{ads}) \quad (11)$$

where R is gas constant, T is absolute temperature and the constant, 55.5 is the molar concentration of water.

The results obtained for the interaction parameter, a, equilibrium constant of adsorption, K_{ads} and change in Gibbs free energy of adsorption, ΔG_{ads} are listed in Table 3. The

Table 3. Interaction Parameter, Equilibrium Adsorption Constant, and Change in Free Energy of Adsorption Obtained from Frumkin Adsorption Isotherm Fitting at 303.15 K

inhibitor	a	K_{ads} ($\times 10^{-5}$ L/mol)	$-(\Delta G_{ads})$ (kJ/mol)
PQDPB	3.530	2.44	41.38
PQDPP	4.818	20.82	46.79
PPQDPE	3.499	2.96	41.87

values of a (the interaction parameter) obtained for the studied inhibitors are all greater than zero, which connotes attraction between the adsorbed inhibitor species. Adsorption of the inhibitors on steel surface is spontaneous as inferred from the negative values of ΔG_{ads}. A value of ΔG_{ads} around −20 kJ/mol or less negative is usually attributed to electrostatic interactions between charged inhibitor molecules and charged metal surface, known as physisorption process, while values around −40 kJ/mol or larger negative values imply that the adsorption process is characterized by charge sharing or transfer from organic molecules to the metal surface to form coordinate bond (i.e., chemisorption process).[55] The values of ΔG_{ads} obtained for the studied compounds are beyond the threshold associated with

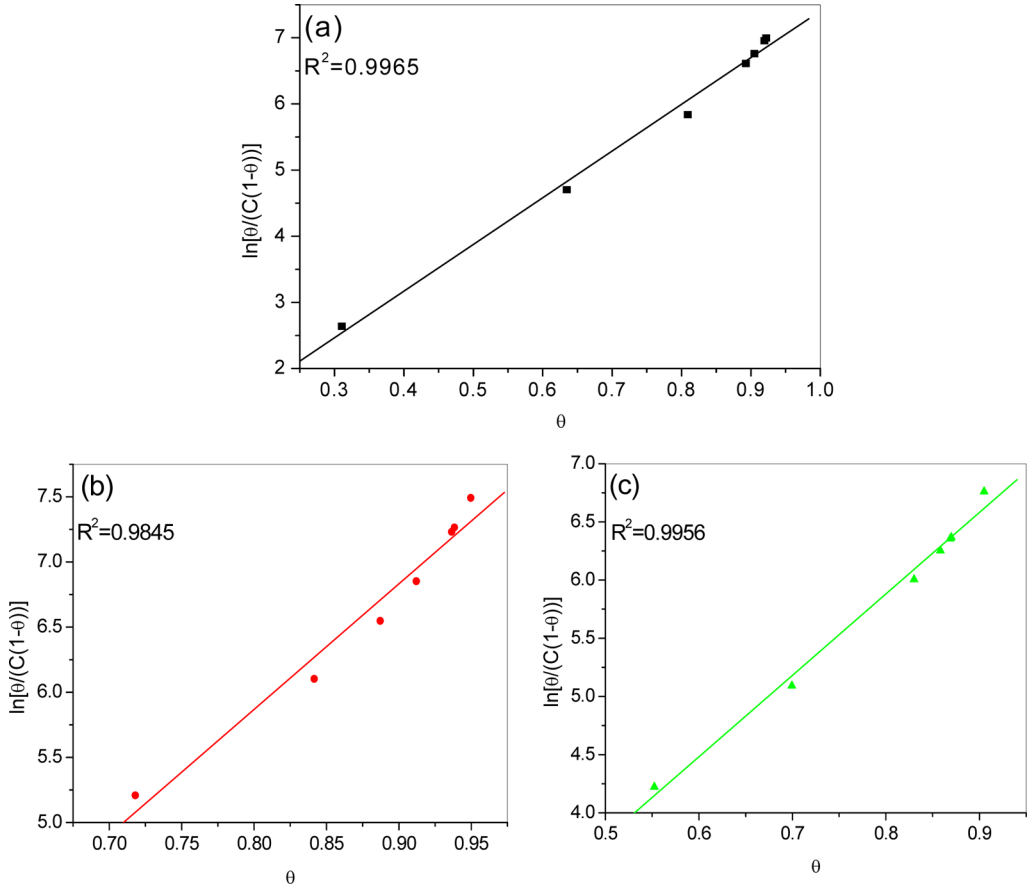

Figure 6. Frumkin isotherm plots for mild steel corrosion in 1 M HCl in the presence of various concentrations of (a) PQDPB, (b) PQDPP, and (c) PPQDPE.

DOI: 10.1021/acs.jpcc.5b03285
J. Phys. Chem. C 2015, 119, 16004−16019

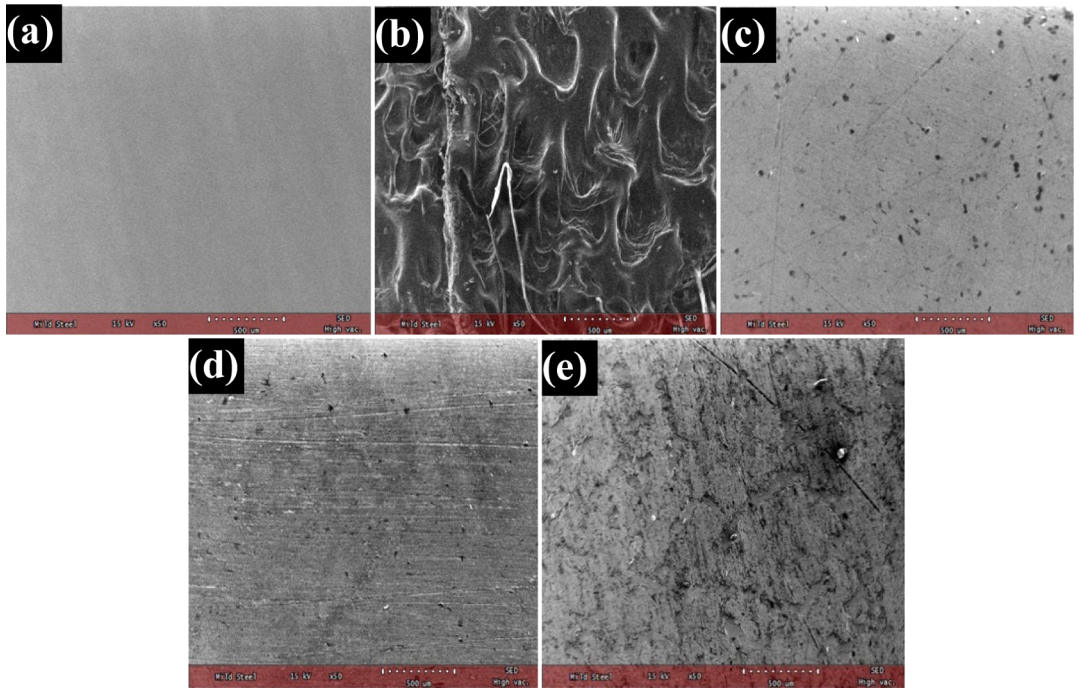

Figure 7. SEM images of mild steel (a) plain mild steel, (b) mild steel in 1 M HCl (blank), (c) PQDPB, (d) PQDPP, and (e) PPQDPE.

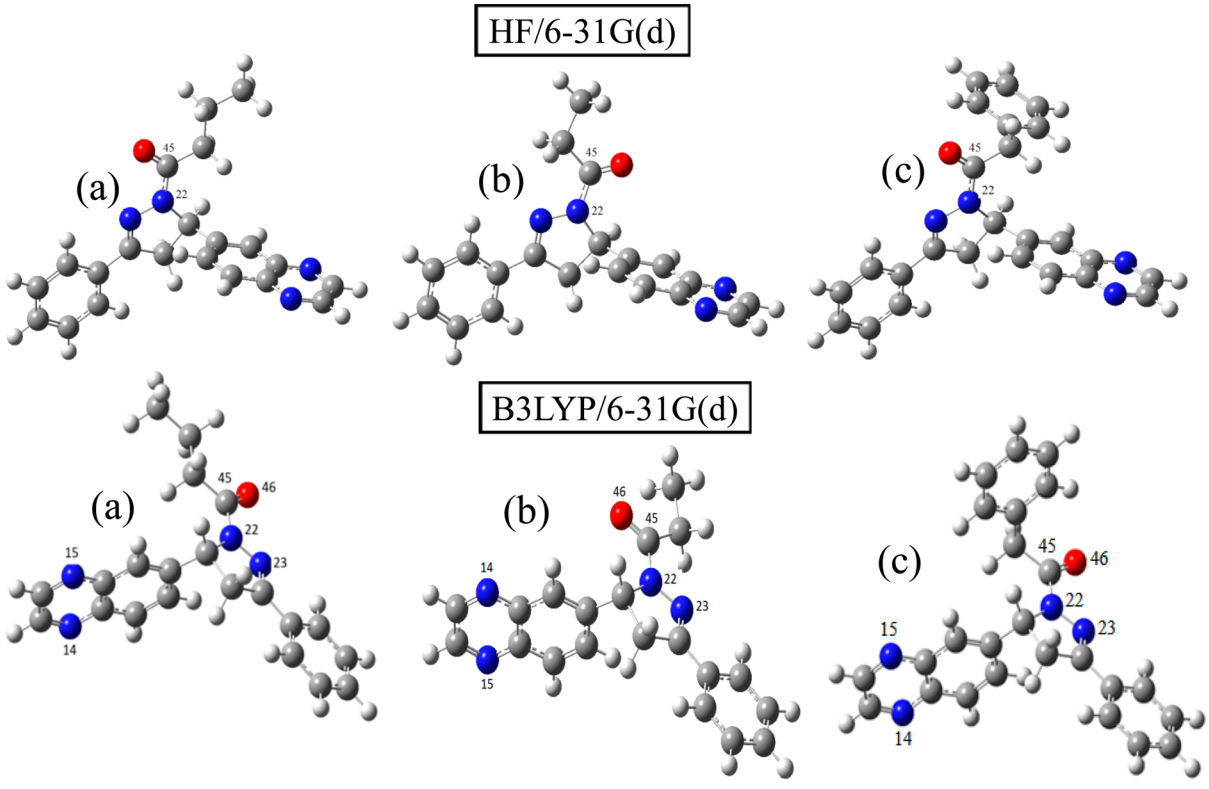

Figure 8. Gas phase optimized structures of the neutral form of (a) PQDPB, (b) PQDPP and (c) PPDQPE at HF/6-31G(d), and B3LYP/6-31G(d) levels.

chemisorption. In other words, the adsorption process of the studied compounds on mild steel surface is mainly characterized by chemisorption processes.[56−58]

3.6. Surface Morphology. Surface morphology of mild steel immersed in the aggressive solution of 1 M HCl without and with maximum concentration of the three inhibitors was carried out using scanning electron microscopy (SEM) technique. SEM images provide information on the surface morphology of the mild steel specimens immersed in each aggressive solution. The extent of surface damage due to corrosion in each medium can be related to the efficiency of the inhibitor. SEM images presented in Figure 7 show that the steel surface is extremely gnawed and eroded as a result of uninhibited corrosion in 1 M HCl (blank) (b) as compared

DOI: 10.1021/acs.jpcc.5b03285
J. Phys. Chem. C 2015, 119, 16004−16019

Table 4. Gas Phase Quantum Chemical Parameters of PQDPB, PQDPP, and PPQDPE at HF/6-31G(d) and B3LYP/6-31G(d)

	HF/6-31G(d)			B3LYP/6-31G(d)		
parameter	PQDPB	PQDPP	PPQDPE	PQDPB	PQDPP	PPQDPE
E_T (eV)	−1099.54	−1060.51	−1251.01	−1106.50	−1067.20	−1258.93
E_{LUMO} (eV)	1.71	2.00	1.70	−2.16	−1.92	−2.17
E_{HOMO} (eV)	−8.30	−8.41	−8.32	−5.80	−5.86	−5.84
$\Delta E_{L\text{-}H}$ (eV)	10.01	10.41	10.02	3.64	3.94	3.67
A (eV)	−1.71	−2.00	−1.70	2.16	1.92	2.17
I (eV)	8.30	8.41	8.32	5.80	5.86	5.84
χ (eV)	3.30	3.20	3.31	3.98	3.89	4.00
η (eV)	5.00	5.20	5.01	1.82	1.97	1.84
ΔN	0.37	0.36	0.37	0.83	0.79	0.82
dipole (Debye)	5.32	4.38	5.38	4.60	3.96	4.66
mol wt (g/mol)	344.16	330.15	392.16	344.16	330.15	392.16

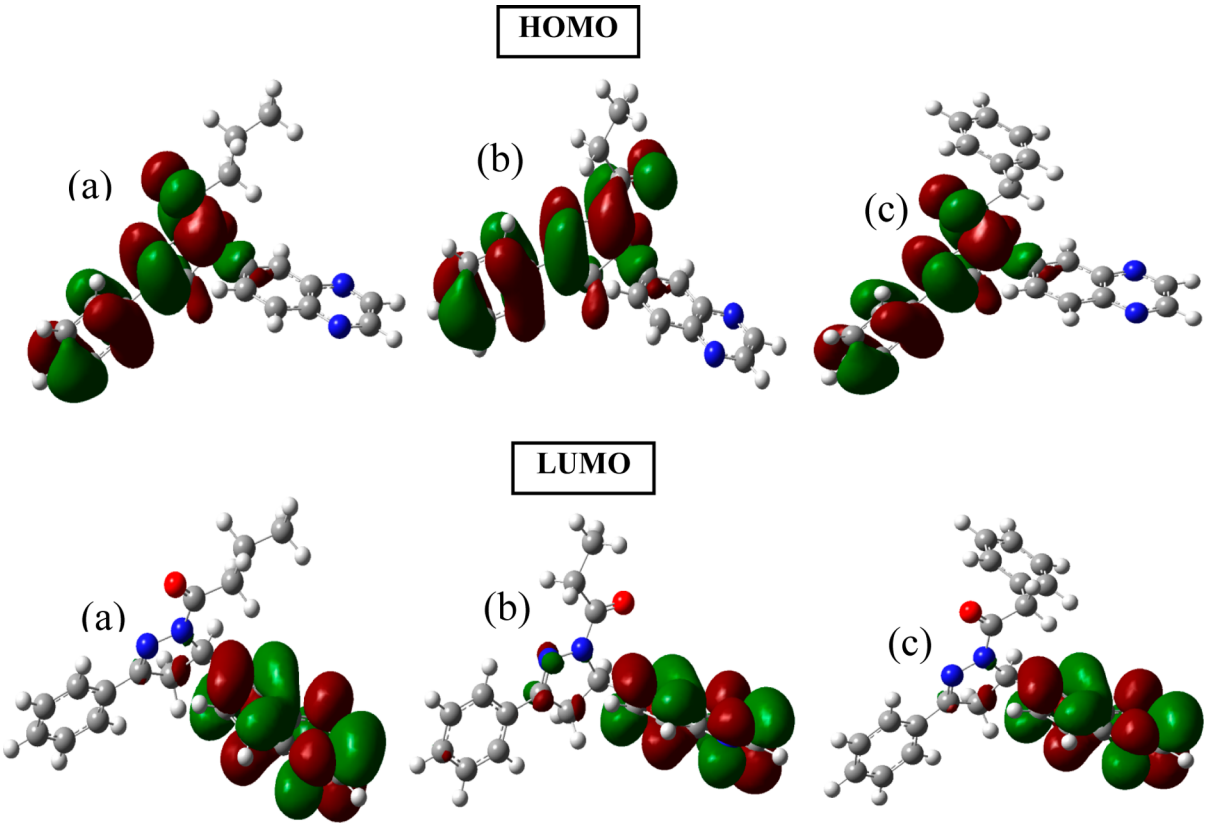

Figure 9. HOMO and LUMO surfaces of the gas phase optimized structures of the neutral form of (a) PQDPB, (b) PQDPP, and (c) PPQDPE at B3LYP/6-31G(d) level.

to plain mild steel (a). Surfaces of mild steel immersed in the systems containing 60 ppm each of PQDPB (c), PQDPP (d), and PPQDPE (e) are not as badly attacked by acid corrosion as they exhibit close resemblance to the freshly polished steel surface. This supports the fact that the inhibitors adsorbed onto mild steel surface and protect the surface from direct attack by the acid.

3.7. Quantum Chemical Calculations. Quantum chemical calculations have been proven useful in explaining the relationship between inhibition efficiency of an organic inhibitor and its molecular/electronic structure. Geometry optimizations of molecular structures of the three inhibitors were carried out in the gas phase without symmetry constraint. Both ab initio Hartree−Fock (HF) and density functional theory (DFT) methods were used in order to ensure adequate explanation of the inhibition properties of the molecules in terms of their molecular and electronic structures. The popular B3LYP functional comprising the Becke three-parameter exchange functional together with Lee−Yang−Parr correlation functional was used for the DFT calculations. The 6-31G* split valence Pople basis set was used for all the calculations. The resulting optimized geometries were confirmed to be of energy minima with the absence of imaginary frequency in the vibrational and force constant calculations. Since the molecules contain multiple donor sites with varying degree of basicity, calculations were also carried out on the protonated forms of the molecules to investigate the possibility of the molecules being protonated in the acid and the likelihood of the steel corrosion being inhibited by the protonated species.

DOI: 10.1021/acs.jpcc.5b03285
J. Phys. Chem. C 2015, 119, 16004−16019

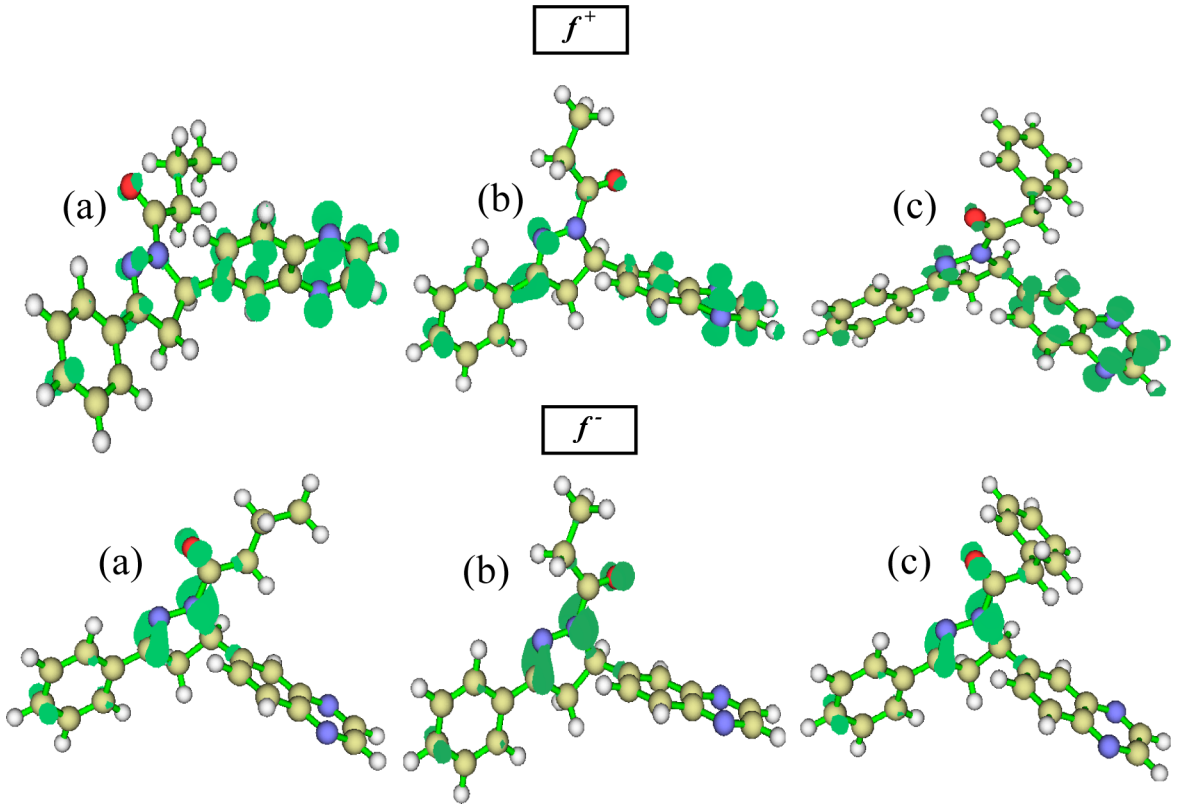

Figure 10. Fukui functions for the neutral form of (a) PQDPB, (b) PQDPP and (c) PPQDPE visualized at 0.003 and 0.005 isosurfaces for f^+ and f^- respectively.

Neutral Species. Optimized structures of the neutral forms of the three compounds are shown in Figure 8 with numbering labels on only the atoms referenced in the Results and Discussions. Relevant quantum chemical parameters of the optimized structures are listed in Table 4. The trends of properties obtained using HF and DFT methods are the same, though the magnitudes of most of the parameters are different (Table 4). This is not unexpected as the levels of approximations employed by the two methods are not the same. For instance, HF/6-31G(d) assigned a partial double bond to the supposed saturated bond between N22 and C45 and seems to overestimate some of the electronic properties.

Adsorption of an inhibitor on a metal surface is often explained based on donor−acceptor relationship between the inhibitor and metal atom. The E_{HOMO} of an inhibitor is associated with its tendency to donate electron(s) to the vacant d-orbitals of the metal atom, while the E_{LUMO} is often related with the propensity of the inhibitor molecule to accept electrons from d-orbitals of the metal. Usually, a higher value of E_{HOMO} implies better chance of forward donation of electrons to metal, and a lower E_{LUMO} favors electron accepting ability of the inhibitor. The energy gap, $\Delta E_{L\text{-}H}$ between HOMO and LUMO is often used as an index of relative reactivity or stability of inhibitor molecule.[59] Graphical surfaces of HOMO and LUMO of the studied compounds are shown in Figure 9. The HOMO surfaces of the three compounds are similar and are distributed along the 3-phenyl-4,5-dihydropyrazole unit, extending to their carbonyl functional groups. Their LUMO surfaces are also similar, being localized mainly on the quinoxaline ring. Apart from total energy (E_T) and molecular weight (molecular weight), most of the other parameters obtained for PQDPB and PPQDPE are amazingly close in magnitudes despite the large difference in their molecular weights. This may inform why the trend of their experimental % IE was not consistent at lower and higher concentrations. As mentioned earlier in sections 3.1 and 3.2, PPQDPE shows better inhibition efficiency than PQDPB at lower concentrations but the trend is reversed at higher concentrations. The number of electrons transferred (ΔN) according to Lukovits et al. (2001)[60] is used to correlate inhibition efficiency of an inhibitor with its electron-donating ability to the metal surface such that, a value of $\Delta N < 3.6$ implies that the inhibition efficiency increases by increasing the electron-donating ability to the metal surface. The values of ΔN in Table 4 are in agreement with Lukovits's study,[25,60] but the trend is not consistent with the experimental inhibition efficiency. There is dissenting opinion in the use of dipole moment as a descriptor for inhibition performance. Some authors are of the opinion that an increase in dipole moment leads to decrease in inhibition efficiency with the explanation that low values of dipole moment will favor accumulation of the inhibitor in the surface layer. In another view, some authors believe that high dipole moment will enhance inhibition efficiency due to increased dipole−dipole interactions between the inhibitor molecules and the metal surface.[61−64] The trend of the dipole moment values for the three inhibitors as shown in Table 4 is in line with the opinion of the authors that believe in increasing inhibition performance with decreasing dipole moment.[61,65,66]

Fukui functions provide information about electrophilic and nucleophilic active sites in organic inhibitors. Electrophilic (f^+) and nucleophilic (f^-) Fukui functions were calculated using the MPA and FD approximations approach. Sites with substantial values of f^+ have tendencies to receive charges from a charged metal surface while sites with substantial values of f^- have

DOI: 10.1021/acs.jpcc.5b03285
J. Phys. Chem. C 2015, 119, 16004−16019

tendencies to donate charges to metal surface. Figure 10 shows the electron density surfaces of f^+ and f^- for the three inhibitors visualized with Multiwfn software.[39,40]

The three inhibitors have many electrophilic and nucleophilic active sites that facilitate their adsorption onto mild steel surface. Atoms in quinoxaline rings are essentially electrophilic sites, while nucleophilic sites include the carbonyl oxygen atoms and nitrogen atoms in dihydropyrazole rings.

The quantum chemical parameters in Table 4 do not give enough justifications to the experimentally observed trends of % IE. For instance, highest value of $\Delta E_{L\text{-}H}$ and η obtained for PQDPP do not correspond with its highest value of experimental % IE. Since these compounds have a number of donor atoms or basic sites, there is a chance that one or more of these sites is/are protonated in the acid such that the steel corrosion is inhibited by the protonated species. Therefore, quantum chemical calculations were also carried out along this view.

Protonated Species. The compounds were protonated singly at N14, N15, N22, N23, and O46. Gas phase geometry optimizations and frequency calculations were carried out on each monoprotonated species at B3LYP/6-31G(d). Since N22 is a saturated nitrogen atom, protonation of this atom was not favorable as it leads to the cleavage of the N22−C45 bond. The most preferred site of protonation in each molecule was determined based on gas phase proton affinity (PA) and basicity (GB) values. Each compound was treated as a potential base with one prospective basic site. Protonation reaction at a particular donor site in a neutral molecule, B can be written as

$$B + H^+ \rightleftharpoons BH^+ \tag{12}$$

Gas phase proton affinity (PA) for eq 12 was calculated as the negative value of the difference in enthalpies of product and reactants, expressed as[67−70]

$$PA = -\Delta H = -[H_{gas}(BH^+) - (H_{gas}(B) + H_{gas}(H^+))] \tag{13}$$

where H_{gas} is the enthalpy at 298.15 K labeled in Gaussian output for frequency calculations as the sum of electronic and thermal enthalpies. Since H^+ is a monatomic species, the only nonzero contribution to its enthalpy is the translational energy ($3/2RT$ = 3.720 kJ/mol). Gas phase basicity of each prospective site of protonation was also calculated as the negative change in Gibbs free energy of the protonation reaction in eq 12 as[70]

$$GB = -\Delta G = G_{gas}(B) + G_{gas}(H^+) - G_{gas}(BH^+) \tag{14}$$

where G_{gas} is the free energy at 298.15 K labeled in Gaussian output for force constant calculations as sum of electronic and thermal free energies. $G_{gas}(H^+)$ is defined as

$$G_{gas}(H^+) = 3/2RT + TS(H^+) \tag{15}$$

where $S(H^+)$ was taken to be 108.95 J/mlo/K.[69,70] Absolute values of PA and GB and their respective relative values (ΔPA and ΔGB) calculated at 298.15 K using the B3LYP/6-31G(d) method are listed in Table 5. The results in Table 5 show that the most probable site of protonation is N23 in PQDPB, N14 in PQDPP and O46 in PPQDPE. More so, there is a chance of multiple protonation in some cases where ΔPA and ΔGB are close to that of the most preferred site of protonation. For instance, PQDPB may as well be protonated at O46, PQDPP may be protonated at all sites, while PPQDPE may also be

Table 5. Relative[a] Values of PA and GB for PQDPB, PQDPP, and PPQDPE at B3LYP/6-31G(d) Level

	PA (kJ/mol)/protonation site				GB (kJ/mol)/protonation site			
compound	N14	N15	N23	O46	N14	N15	N23	O46
PQDPB	926.59 (−39.46)	924.12 (−41.92)	966.04 (0)	954.24 (−11.80)	958.93 (−42.13)	956.88 (−44.18)	1001.06 (0)	985.50 (−15.56)
PQDPP	949.06 (0)	942.36 (−6.69)	939.81 (−9.25)	942.40 (−6.65)	980.27 (0)	975.92 (−4.35)	972.61 (−7.66)	973.83 (−6.44)
PPQDPE	918.39 (−52.55)	916.38 (−54.56)	959.22 (−11.72)	970.94 (0)	954.12 (−48.95)	953.07 (−50.00)	996.75 (−6.32)	1003.07 (0)

[a]In parentheses: ΔPA = PA(less stable) − PA(most stable); ΔGB = GB(less stable) − GB(most stable).

DOI: 10.1021/acs.jpcc.5b03285
J. Phys. Chem. C 2015, 119, 16004−16019

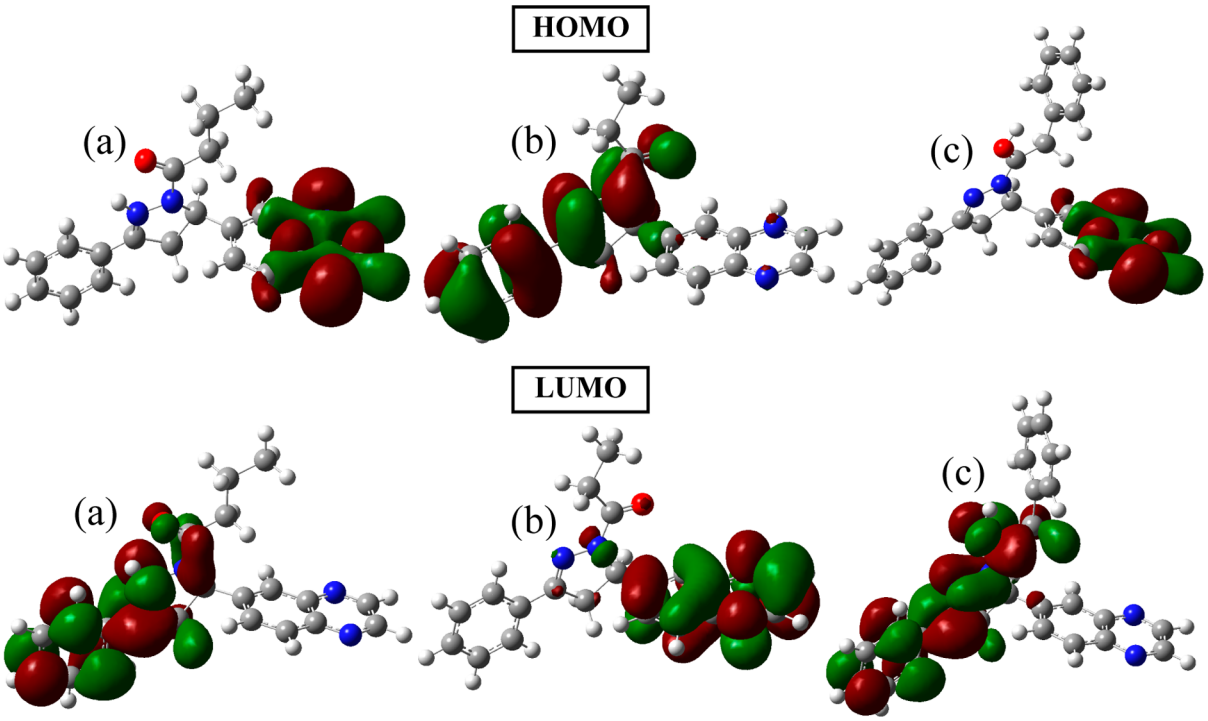

Figure 11. HOMO and LUMO surfaces of the gas phase optimized structures of the most stable protonated form of (a) PQDPB, (b) PQDPP, and (c) PPQDPE at B3LYP/6-31G(d) level.

protonated at N23 under favouble conditions. Again, PQDPB and PPQDPE exhibit similar behavior in terms of preferred sites of protonation as both can readily be protonated at N23 and O46, though the most preferred site selectivity is reversed. It is observed that PPQDPE has a better chance of getting doubly protonated than PQDPB. There is therefore a possibility of this compound getting doubly protonated at lower concentrations (10 and 20 ppm), making it to exhibit higher inhibition efficiencies at these concentrations than PQDPB. However, when PQDPB happens to be double protonated (especially at higher concentrations: 40 and 60 ppm), it shows better inhibition potency than PPQDPE. For further explanation, relative reactivity of the most stable protonated species was investigated using the frontier molecular orbital (FMO) parameters. The HOMO and LUMO graphical surfaces of the most stable protonated species are shown in Figure 11 and the corresponding relevant quantum chemical parameters are listed in Table 6. The results in Table 6 show that PQDPP−$H^+_{(N14)}$ has the highest E_{HOMO}, E_{LUMO} and the lowest $\Delta E_{L\text{-}H}$ when compared with PQDPB-$H^+_{(N23)}$ and PPQDPE-$H^+_{(O46)}$.The trends of these parameters are

$$E_{HOMO}\text{: PQDPP}-H^+_{(N14)} > \text{PQDPB}-H^+_{(N23)} \geq \text{PPQDPE}-H^+_{(O46)}$$

$$E_{LUMO}\text{: PQDPP}-H^+_{(N14)} < \text{PQDPB}-H^+_{(N23)} < \text{PPQDPE}-H^+_{(O46)}$$

Table 6. Quantum Chemical Parameters for the Most Stable Protonated Species: PQDPB−H^+, PQDPP−H^+, and PPQDPE−H^+

	B3LYP/6-31G(d)		
parameter	PQDPB	PQDPP	PPQDPE
E_T (eV)	−1106.88	−1067.57	−1259.31
E_{LUMO} (eV)	−6.20	−7.05	−5.17
E_{HOMO} (eV)	−9.25	−8.35	−9.28
$\Delta E_{L\text{-}H}$ (eV)	3.05	1.30	4.11
A (eV)	6.20	7.05	5.17
I (eV)	9.25	8.35	9.28
χ (eV)	7.72	7.70	7.22
η (eV)	1.52	0.65	3.61
ΔN	−0.24	−0.54	−0.03
dipole (Debye)	8.31	12.90	3.61

$$\Delta E_{L-H}\text{: PQDPP}-H^+_{(N14)} < \text{PQDPB}-H^+_{(N23)} < \text{PPQDPE}-H^+_{(O46)}$$

These trends are in perfect support of PQDPP as the most efficient inhibitor (cf. experimental % IE values). PQDPP−$H^+_{(N14)}$ also has the least value of chemical hardness (η), which also supports its high reactivity and enhanced inhibition performance. The negative value of ΔN for the protonated species is due to their higher electronegativity than atomic iron. This suggests back-donation from the d-orbitals of iron to the vacant π-molecular orbitals of the protonated inhibitor molecule. The values of ΔN suggest that PQDPP−$H^+_{(N14)}$ has the highest tendency to receive electrons from the metal during retro-donation and the trend supports experimental inhibition performance. The trend of the dipole moments of the protonated species is in line with previous reports that believe that the higher the dipole moment the higher the

DOI: 10.1021/acs.jpcc.5b03285
J. Phys. Chem. C 2015, 119, 16004−16019

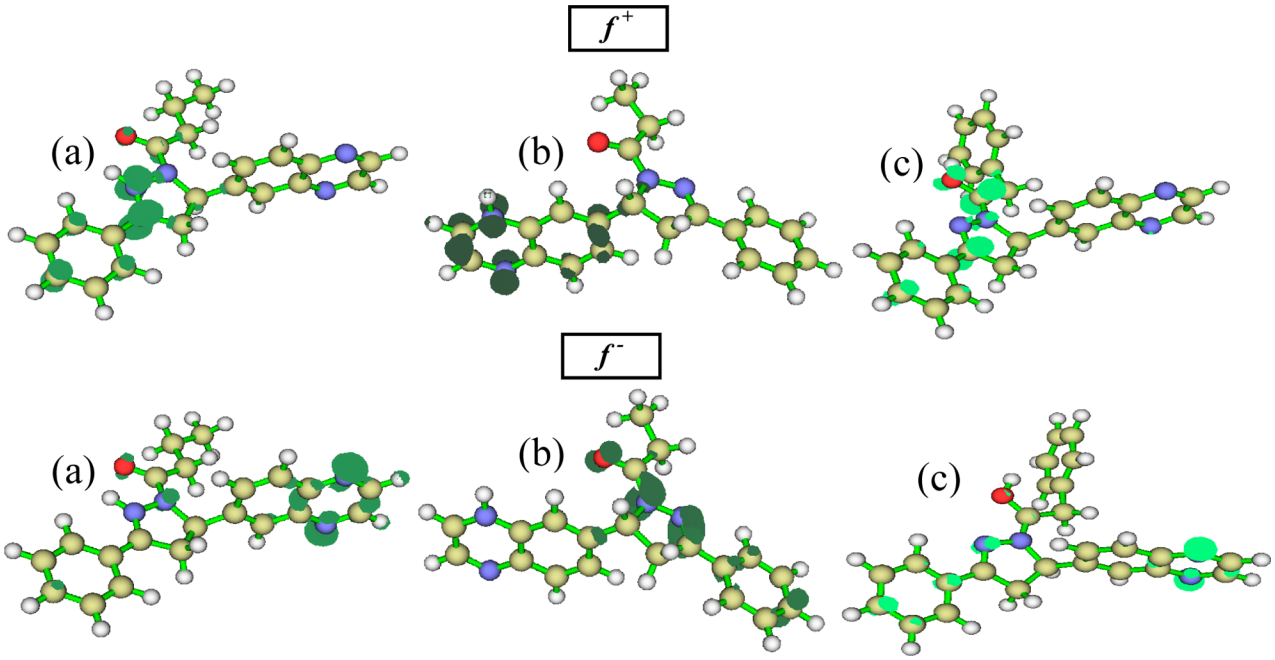

Figure 12. Fukui functions for the most stable protonated form of (a) PQDPB, (b) PQDPP and (c) PPQDPE visualized at 0.003 and 0.005 isosurfaces for f^+ and f^- respectively.

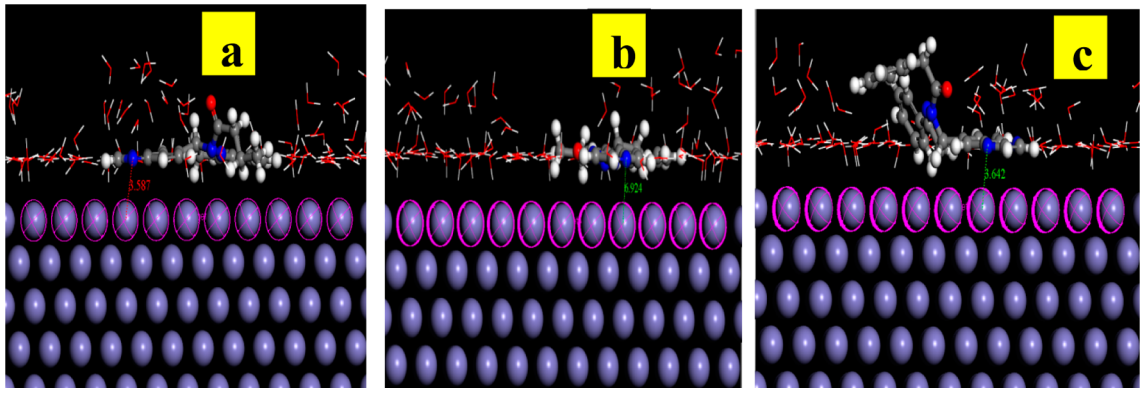

Figure 13. Most stable low energy configuration for the adsorption of (a) PQDPB, (b) PQDPP, and (c) PPQDPE on Fe (110)/100 H_2O interface obtained through the Monte Carlo simulations.

Table 7. Outputs and Descriptors Calculated by the Monte Carlo Simulation for the Lowest Adsorption Configurations of PQDPB, PQDPP, and PPQDPE on Fe(110)/100H_2O Interface (in kJ/mol)

systems	total energy	adsorption energy	rigid adsorption energy	deformation energy	$dE_{ad}/dN_{i\ \text{inhibitors}}$	$dE_{ad}/dN_{i\ H_2O}$
Fe(110)/PQDPB/100 H_2O	−6381.69	−6651.97	−6942.97	290.96	−777.09	−27.78
Fe(110)/PQDPP/100 H_2O	−6514.32	−6815.53	−7146.90	331.33	−833.41	−54.81
Fe(110)/PPQDPE/100 H_2O	−6374.70	−6649.76	−6950.46	300.66	−691.03	−26.28

inhibition efficiency. The Fukui indices of the protonated inhibitors are also calculated and the graphical electron density surfaces are presented in Figure 12.

3.8. Monte Carlo Simulations Results. The most stable adsorption configurations of (a) PQDPB, (b) PQDPP, and (c) PPQDPE on Fe(110) surface in the presence of 100 water molecules was simulated using Monte Carlo simulations and is shown in Figure 13. The corresponding values for the outputs and descriptors are listed in Table 7. The parameters include total energy of the substrate−adsorbate configuration, which is defined as the sum of the energies of the adsorbate components, the rigid adsorption energy, and the deformation energy. The substrate energy (i.e., Fe(110) surface) is taken as zero. Moreover, adsorption energy reports the energy released (or required) when the relaxed adsorbate component was adsorbed on the substrate. The adsorption energy is defined as the sum of the rigid adsorption energy and the deformation energy for the adsorbate component. The rigid adsorption energy reports the energy released (or required) when the unrelaxed adsorbate component (before the geometry optimization step) was adsorbed on the substrate. The deformation energy reports the energy released when the adsorbed adsorbate component was relaxed on the substrate surface. Finally, (dE_{ad}/dN_i) reports the energy of substrate−adsorbate

DOI: 10.1021/acs.jpcc.5b03285
J. Phys. Chem. C 2015, 119, 16004−16019

configurations where one of the adsorbate components has been removed.

From Figure 13, it is evident that PQDPP which exhibited the strongest interaction and by extension highest inhibition efficiency lie flat and completely parallel on the Fe(110) surface leading to a stronger interaction. PQDPB and PPQDPE had various slanting angle of deviations as they interact with the iron surface. This leads to reduced interactions with the iron surface.

It is quite clear from the results obtained from Table 7 that PQDPP the adsorption energies of the studied inhibitors on iron surface increased in the order: PQDPP > PQDPB > PPQDPE. Highest negative adsorption energy indicates the system with the most stable and stronger adsorption.[71,72] The trend is in agreement with the results of inhibition efficiency obtained experimentally for the investigated inhibitors. In all cases, the adsorption energies of the inhibitors are far higher than that of water molecules (Table 7). This indicates the possibility of gradual substitution of water molecules from the surface of iron surface resulting in the formation of a stable layer which can protect the iron from aqueous corrosion.

3.9. Inhibition Activity and Carbonyl Reactivity. Since the three inhibitors studied in the present work only differ in carbonyl chain lengths, it may be necessary to consider possible correlations between the trends of inhibition efficiency and carbonyl reactivity. The reactivity of carbonyl group arises from the electronegativity of oxygen atom and the resulting polarization of the carbon−oxygen double bond. Aldehydes are generally more reactive than ketones on the basis of electronic and steric effects. In other words, short-chain carbonyls are more reactive than long-chain carbonyls. More so, aliphatic carbonyls are more reactive than aromatic carbonyls because the electron-donating resonance effect of the aromatic ring in aromatic carbonyls makes the carbonyl group less electrophilic than the carbonyl group of an aliphatic carbonyl.[73] The results obtained for the *% IE* of the studied inhibitors agree with the trend of reactivity of carbonyl compounds. PQDPP with the shortest carbonyl chain length is the most efficient inhibitor of mild steel corrosion in 1 M HCl.

3.9. Conclusions. Three quinoxaline derivatives with different chain length of carbonyl functional groups were studied for their inhibition characteristics on mild steel corrosion in 1 M HCl using both experimental and theoretical techniques. The following conclusions were drawn from the studies:

1. Both polarization and EIS studies revealed that the three compounds are good inhibitors of mild steel corrosion in 1 M HCl and the polarization study shows that the compounds are all mixed-type inhibitors.
2. Adsorption of the studied inhibitors is spontaneous, essentially chemisorption and obey the Frumkin adsorption isotherm.
3. SEM images show that the inhibitors adsorb on mild steel surface and protect the steel surface against acid attack.
4. Quantum chemical calculations revealed that the inhibitors have high proton affinity in acidic medium and the results agree with experimental data.
5. The results of the Monte Carlo simulations accord with the experimentally determined inhibition efficiencies of the inhibitors, i.e. PQDPP > PQDPB > PPQDPE.
6. PQDPP with the shortest carbonyl substituent having the least steric hindrance showed the best inhibition efficiency.

AUTHOR INFORMATION

Corresponding Author

*(E.E.E.) E-mail: Eno.Ebenso@nwu.ac.za. Telephone: +27 183892050/2051. Fax: +27183892052.

Notes

The authors declare no competing financial interest.

ACKNOWLEDGMENTS

L.O.O acknowledges the NRF/Sasol Inzalo foundation for support towards his Ph.D. studies. E.E.E acknowledges financial support from NRF (South Africa) for incentive funding for rated researchers. I.B.O is grateful to the Center of Research Excellence in Corrosion, King Fahd University of Petroleum and Minerals (KFUPM), for support.

REFERENCES

(1) Pinchuk, S.; Gubenko, S.; Belaya, E. Correlation between Electrochemical Corrosion and Structural State of Steel by Simulation of Operation Conditions of Railway Wheels. *Chem. Chem. Technol.* **2010**, *4*, 151−158.

(2) Gajek, A.; Zakroczymski, T.; Romanchuk, V.; Topilnytsky, P. Protective Properties and Spectral Analysis of Nitrogen- and Oxygen-Containing Corrosion Inhibitors for Oil Equipment. *Chem. Chem. Technol* **2012**, *6*, 209−217.

(3) de la Fuente, D.; Diaz, I.; Simancas, J.; Chico, B.; Morcillo, M. Long-term Atmospheric Corrosion of Mild Steel. *Corros. Sci.* **2011**, *53*, 604−617.

(4) Ulaeto, S. B.; Ekpe, U. J.; Chidiebere, M. A.; Oguzie, E. E. Corrosion Inhibition of Mild Steel in Hydrochloric Acid by Acid Extracts of *Eichhornia Crassipes*. *Int. J. Mater. Chem.* **2012**, *2*, 158−164.

(5) Khaled, K. F. New Synthesized Guanidine Derivative as a Green Corrosion Inhibitor for Mild Steel in Acidic Solutions. *Int. J. Electrochem. Sci.* **2008**, *3*, 462−475.

(6) Lebrini, M.; Lagrenee, A.; Traisnel, A.; Gengembre, L.; Vezin, H.; Bentiss, F. Enhanced Corrosion Resistance of Mild Steel in Normal Sulfuric Acid Medium by 2,5-bis(*n*-thienyl)-1,3,4-thiadiazoles: Electrochemical, X-ray Photoelectron Spectroscopy and Theoretical Studies. *Appl. Surf. Sci.* **2007**, *253*, 9267−9276.

(7) Guzman-Lucero, D.; Olivares-Xometl, O.; Martinez-Palou, R.; Likhanova, N. V.; Dominguez-Aguilar, M. A.; Garibay-Febles, V. Synthesis of Selected Vinylimidazolium Ionic Liquids and their Effectiveness as Corrosion Inhibitors for Carbon Steel in Aqueous Sulfuric Acid. *Ind. Eng. Chem. Res.* **2011**, *50*, 7129−7140.

(8) Ebenso, E. E.; Arslan, T.; Kandemirli, F.; Love, I.; Gretir, C. O.; Saracoglu, M.; Umoren, S. A. Theoretical Studies of Some Sulphonamides as Corrosion Inhibitors for Mild Steel in Acidic Medium. *Int. J. Quantum Chem.* **2010**, *110*, 2614−2636.

(9) Ehsani, A.; Mahjani, M. G.; Moshrefi, R.; Mostaanzadeha, H.; Shayehb, J. S. Electrochemical and DFT Study on the Inhibition of 316L Stainless Steel Corrosion in Acidic Medium by 1-(4-nitrophenyl)-5-amino-1*H*-tetrazole. *RSC Adv.* **2014**, *4*, 20031−20037.

(10) Murulana, L. C.; Singh, A. K.; Shukla, S. K.; Kabanda, M. M.; Ebenso, E. E. Experimental and Quantum Chemical Studies of Some Bis(trifluoromethyl-sulfonyl) Imide Imidazolium-Based Ionic Liquids as Corrosion Inhibitors for Mild Steel in Hydrochloric Acid solution. *Ind. Eng. Chem. Res.* **2012**, *51*, 13282−13299.

(11) Bailly, C.; Echepare, S.; Gago, F.; Waring, M. J. Recognition Elements that Determine Affinity and Sequence-Specific Binding to DNA of 2QN, A Biosynthetic Bis-Quinoline Analogue of Echinomycin. *Anti-Cancer Drug Des.* **1999**, *14*, 291−303.

DOI: 10.1021/acs.jpcc.5b03285
J. Phys. Chem. C 2015, 119, 16004−16019

(12) Obot, I. B.; Obi-Egbedi, N. O. Indeno-1-one-[2,3-b]-quinoxaline as an Effective Inhibitor for the Corrosion of Mild Steel in 0.5 M H_2SO_4 Solution. *Mater. Chem. Phys.* **2010**, *122*, 325−328.
(13) Thomas, K. R. J.; Tyagi, P. Synthesis, Spectra, and Theoretical Investigations of the Triarylamines Based on 6*H*-Indolo-[2,3-*b*]-quinoxaline. *J. Org. Chem.* **2010**, *75*, 8100−8111.
(14) Geethavan, M.; Reddy, J. R.; Sathyanarayana, S. V. Synthesis, Antimicrobial and Wound Healing Activities of Diphenylquinoxaline Derivatives. *Int. J. Pharm. Technol.* **2012**, *4*, 4700−4710.
(15) Obot, I. B.; Obi-Egbedi, N. O.; Odozi, N. W. Acenaphtho-[1,2-b]-quinoxaline as a Novel Corrosion Inhibitor for Mild Steel in 0.5 M H_2SO_4. *Corros. Sci.* **2010**, *52*, 923−926.
(16) Zarrouk, A.; Zarrok, H.; Salghi, R.; Hammouti, B.; Al-Deyab, S. S.; Touzani, R.; Bouachrine, M.; Warad, I.; Hadda, T. B. A Theoretical Investigation on the Corrosion Inhibition of Copper by Quinoxaline Derivatives in Nitric Acid Solution. *Int. J. Electrochem. Sci.* **2012**, *7*, 6353−6364.
(17) El-Hajjaji, F.; Zerga, B.; Sfaira, M.; Taleb, M.; Ebn Touhami, M.; Hammouti, B.; Al-Deyab, S. S.; Benzeid, H.; El, M. Essassi Comparative Study of Novel N-Substituted Quinoxaline Derivatives towards Mild Steel Corrosion in Hydrochloric Acid: Part 1. *J. Mater. Environ. Sci.* **2014**, *5* (Y), 255−262.
(18) Benabdellah, M.; Touzani, R.; Aouniti, A.; Dafali, A.; Elkadiri, S.; Hammouti, B.; Benkaddour, M. Investigation of the Inhibitive Effect of Some Quinoxaline Compounds on the Corrosion of Steel in HCl Solution. *Phys. Chem. News* **2007**, *37*, 63−69.
(19) Benabdellah, M.; Tebbji, K.; Hammouti, B.; Touzani, R.; Aouniti, A.; Dafali, A.; El Kadiri, S. The Effect of Temperature on the Corrosion of Steel in 1M HCl in the Presence of Quinoxaline Compound. *Phys. Chem. News* **2008**, *43*, 115−120.
(20) Zarrouk, A.; Dafali, A.; Hammouti, B.; Zarrok, H.; Boukhris, S.; Zertoubi, M. Synthesis, Characterization and Comparative Study of Functionalized Quinoxaline Derivatives towards Corrosion of Copper in Nitric Acid Medium. *Int. J. Electrochem. Sci.* **2010**, *5*, 46−55.
(21) El Ouali, I.; Hammouti, B.; Aouniti, A.; Ramli, Y.; Azougagh, M.; Essassi, E. M.; Bouachrine, M. Thermodynamic Characterisation of Steel Corrosion in HCl in the Presence of 2-phenylthieno-(3, 2-b)-quinoxaline. *J. Mater. Environ. Sci.* **2010**, *1* (N), 1−8.
(22) Hammouti, B.; Zarrouk, A.; AL-Deyab, S. S.; Warad, I. Temperature Effect, Activation Energies and Thermodynamics of Adsorption of Ethyl-2-(4-(2-ethoxy-2-oxoethyl)-2-p-tolylquinoxalin-1(4H)-yl) Acetate on Cu in HNO_3. *Orient. J. Chem.* **2011**, *27*, 23−31.
(23) Elayyachy, M.; Hammouti, B.; El Idrissi, A.; Aounit, A. Adsorption and Corrosion Inhibition Behavior of C38 Steel by One Derivative of Quinoxaline in 1 M HCl. *Port. Electrochim. Acta* **2011**, *29*, 57−68.
(24) Fu, J. J.; Zang, H. S.; Wang, Y.; Li, S. N.; Chen, T.; Liu, X. D. Experimental and Theoretical Study on the Inhibition Performances of Quinoxaline and Its Derivatives for the Corrosion of Mild Steel in Hydrochloric Acid. *Ind. Eng. Chem. Res.* **2012**, *51*, 6377−6386.
(25) Zarrouk, A.; Hammouti, B.; Dafali, A.; Bouachrine, M.; Zarrok, H.; Boukhris, S.; Al-Deyab, S. S. A Theoretical Study on the Inhibition Efficiencies of Some Quinoxalines as Corrosion Inhibitors of Copper in Nitric Acid. *J. Saudi Chem. Soc.* **2014**, *18*, 450−455.
(26) Adardour, K.; Touir, R.; Ramli, Y.; Belakhmima, R. A.; Ebn Touhami, M.; Mubengayi, C. K.; El Kafsaoui, H.; Essassi, E. M. Comparative Inhibition Study of Mild Steel Corrosion in Hydrochloric Acid by New Class Synthesised Quinoxaline Derivatives: Part I. *Res. Chem. Intermed.* **2013**, *39*, 1843−1855.
(27) Tang, Y.; Yang, X.; Yang, W.; Wan, R.; Chen, Y.; Yin, X. A Preliminary Investigation of Corrosion Inhibition of Mild Steel in 0.5 M H_2SO_4 by 2-Amino-5-(*N*-Pyridyl)-1,3,4-thiadiazole: Polarization, EIS and Molecular Dynamics Simulations. *Corros. Sci.* **2010**, *52*, 1801−1808.
(28) Khaled, K. F. Molecular Simulation, Quantum Chemical Calculations and Electrochemical Studies for Inhibition of Mild Steel by Triazoles. *Electrochim. Acta* **2008**, *53*, 3484−3492.
(29) Tang, Y.; Yang, X.; Yang, W.; Chen, Y.; Wan, R. Experimental and Molecular Dynamics Studies on Corrosion Inhibition of Mild Steel by 2-amino-5-phenyl-1,3,4-thiadiazole. *Corros. Sci.* **2010**, *52*, 242−249.
(30) Khaled, K. F.; Amin, M. A. Corrosion Monitoring of Mild Steel in Sulphuric Acid Solutions in Presence of Some Thiazole Derivatives − Molecular Dynamics, Chemical and Electrochemical Studies. *Corros. Sci.* **2009**, *51*, 1964−1975.
(31) Musa, A. Y.; Jalgham, R. T. T.; Mohamad, A. B. Molecular Dynamic and Quantum Chemical Calculations for Phthalazine Derivatives as Corrosion Inhibitors of Mild Steel in 1 M HCl. *Corros. Sci.* **2012**, *56*, 176−183.
(32) Khaled, K. F. Monte Carlo Simulations of Corrosion Inhibition of Mild Steel in 0.5 M Sulphuric Acid by Some Green Corrosion Inhibitors. *J. Solid State Electrochem.* **2009**, *13*, 1743−1756.
(33) Gomez, B.; Likhanova, N. V.; Dominguez, M. A.; Martinez-Palou, R.; Vela, A.; Gazquez, J. L. Quantum Chemical Study of the Inhibitive Properties of 2-Pyridyl-Azoles. *J. Phys. Chem. B* **2006**, *110*, 8928−8934.
(34) Frisch, M. J.; Trucks, G. W.; Schlegel, H. B.; Scuseria, G. E.; Robb, M. A.; Cheeseman, J. R.; Scalmani, G.; Barone, V.; Mennucci, B.; Petersson, G. A.; et al. *Gaussian 09*, Revision D.01; Gaussian, Inc.: Wallingford CT, 2009.
(35) Koopmans, T. Über die Zuordnung von Wellenfunktionen und Eigenwerten zu den Einzelnen Elektronen Eines Atoms. *Physica* **1934**, *1*, 104−113.
(36) Martinez, S. Inhibitory Mechanism of Mimosa Tannin Using Molecular Modeling and Substitutional Adsorption Isotherms. *Mater. Chem. Phys.* **2003**, *77*, 97−102.
(37) Pearson, R. G. Absolute Electronegativity and Hardness: Application to Inorganic Chemistry. *Inorg. Chem.* **1988**, *27*, 734−740.
(38) Yang, W.; Mortier, W. J. The Use of Global and Local Molecular Parameters for the Analysis of the Gas-Phase Basicity of Amines. *J. Am. Chem. Soc.* **1986**, *108*, 5708−5711.
(39) Lu, T.; Chen, F. Multiwfn: A Multifunctional Wavefunction Analyzer. *J. Comput. Chem.* **2012**, *33*, 580−592.
(40) Lu, T.; Chen, F. Quantitative Analysis of Molecular Surface Based on Improved Marching Tetrahedra Algorithm. *J. Mol. Graphics Modell.* **2012**, *38*, 314−323.
(41) Kr. Saha, S.; Dutta, A.; Ghosh, P.; Sukul, D.; Banerjee, P. Adsorption and Corrosion Inhibition Effect of Schiff Base Molecules on the Mild Steel Surface in 1 M HCl Medium: A Combined Experimental and Theoretical Approach. *Phys. Chem. Chem. Phys.* **2015**, *17*, 5679−5690.
(42) John, S.; Kuruvilla, M.; Joseph, A. Adsorption and Inhibition Effect of Methyl Carbamate on Copper Metal in 1 N HNO3: An Experimental and Theoretical Study. *RSC Adv.* **2013**, *3*, 8929−8938.
(43) Zhihua, T.; Shengtao, Z.; Weihua, L.; Baorong, H. Adsorption and Inhibitory Mechanism of 1*H*-1,2,4-Triazol-l-yl-methyl-2-(4-chlorophenoxy) Acetate on Corrosion of Mild Steel in Acidic Solution. *Ind. Eng. Chem. Res.* **2011**, *50*, 6082−6088.
(44) Daoud, D. T.; Douadi, T.; Issaadi, S.; Chafaa, S. Adsorption and Corrosion Inhibition of New Synthesized Thiophene Schiff Base on Mild Steel X52 in HCl and H_2SO_4 Solutions. *Corros. Sci.* **2014**, *79*, 50−58.
(45) Lagrenee, M.; Mernari, B.; Bouanis, M.; Traisnel, M.; Bentiss, F. Study of the Mechanism and Inhibiting Efficiency of 3,5-bis(4-methylthiophenyl)-4H-1,2,4-triazole on Mild Steel Corrosion in Acidic Media. *Corros. Sci.* **2002**, *44*, 573−588.
(46) Singh, A. K.; Quraishi, M. A. Effect of Cefazolin on the Corrosion of Mild Steel in HCl Solution. *Corros. Sci.* **2010**, *52*, 152−160.
(47) Farag, A. A.; Ali, T. A. The Enhancing of 2-pyrazinecarboxamide Inhibition Effect on the Acid Corrosion of Carbon Steel in Presence of Iodide Ions. *J. Ind. Eng. Chem.* **2015**, *21*, 627−634.
(48) Hussin, M. H.; Kassim, M. J. Electrochemical, Thermodynamic and Adsorption Studies of (+)-Catechin Hydrate as Natural Mild Steel Corrosion Inhibitor in 1 M HCl. *Int. J. Electrochem. Sci.* **2011**, *6*, 1396−1414.

DOI: 10.1021/acs.jpcc.5b03285
J. Phys. Chem. C 2015, 119, 16004−16019

(49) Ehsani, A.; Babaei, F.; Nasrollahzadeh, M. Electrosynthesis and Absorbance Spectra of TiO_2 Nanoparticles Dispersed in the Conductive Polymer. *Appl. Surf. Sci.* **2013**, *283*, 1060−1064.
(50) Sudheer; Quraishi, M. A. 2-amino-3,5-dicarbonitrile-6-thio-pyridines: New and Effective Corrosion Inhibitors for Mild Steel in 1 M HCl. *Ind. Eng. Chem. Res.* **2014**, *53*, 2851−2859.
(51) Outirite, M.; Lagrenee, M.; Lebrini, M.; Traisnel, M.; Jama, C.; Vezin, H.; Bentiss, F. AC Impedance, X-ray Photoelectron Spectroscopy and Density Functional Theory Studies of 3,5-bis(*n*-pyridyl)-1,2,4-oxadiazoles as Efficient Corrosion Inhibitors for Carbon Steel Surface in Hydrochloric Acid Solution. *Electrochim. Acta* **2010**, *55*, 1670−1681.
(52) John, S.; Joseph, A. Effective Inhibition of Mild Steel Corrosion in 1 M Hydrochloric Acid Using Substituted Triazines: An Experimental and Theoretical Study. *RSC Adv.* **2012**, *2*, 9944−9951.
(53) Dukhin, S. S.; Kretzschmar, G.; Miller, R. *Dynamics of Adsorption at Liquid Interfaces: Theory, Experiment, Application*; Elsevier Sci. B. V.: Amsterdam, The Netherlands, 1995.
(54) Vracar, Lj. M.; Drazic, D. M. Adsorption and Corrosion Inhibitive Properties of Some Organic Molecules on Iron Electrode in Sulfuric Acid. *Corros. Sci.* **2002**, *44*, 1669−1680.
(55) Zhang, X.; Zheng, Y.; Wang, X.; Yan, Y.; Wu, W. Corrosion Inhibition of N80 Steel Using Novel Diquaternary Ammonium Salts in 15% Hydrochloric Acid. *Ind. Eng. Chem. Res.* **2014**, *53*, 14199−14207.
(56) Hmamou, D. B.; Salghi, R.; Zarrouk, A.; Aouad, M. R.; Benali, O.; Zarrok, H.; Messali, M.; Hammouti, B.; Kabanda, M. M.; Bouachrine, M.; et al. Weight Loss, Electrochemical, Quantum Chemical Calculation, and Molecular Dynamics Simulation Studies on 2-(Benzylthio)-1,4,5-triphenyl-1H-imidazole as an Inhibitor for Carbon Steel Corrosion in Hydrochloric Acid. *Ind. Eng. Chem. Res.* **2013**, *52*, 14315−14327.
(57) Yurt, A.; Balaban, A.; Kandemir, S. U.; Bereket, G.; Erk, B. Investigation on Some Schiff Bases as HCl Corrosion Inhibitors for Carbon Steel. *Mater. Chem. Phys.* **2004**, *85*, 420−426.
(58) Li, X.; Deng, S.; Fu, H.; Li, T. Adsorption and Inhibition Effect of 6-benzylaminopurine on Cold Rolled Steel in 1.0 M HCl. *Electrochim. Acta* **2009**, *54*, 4089−4098.
(59) Obot, I. B.; Umoren, S. A.; Gazem, Z. M.; Suleiman, R.; El Ali, B. Theoretical Prediction and Electrochemical Evaluation of Vinylimidazole and Allylimidazole as Corrosion Inhibitors for Mild Steel in 1 M HCl. *J. Ind. Eng. Chem.* **2015**, *21*, 1328−1339.
(60) Lukovits, I.; Kálmán, E.; Zucchi, F. Corrosion Inhibitors-Correlation between Electronic Structure and Efficiency. *Corrosion* **2001**, *57*, 3−8.
(61) Soltani, N.; Behpour, M.; Oguzie, E. E.; Mahluji, M.; Ghasemzadeh, M. A. Pyrimidine-2-thione Derivatives as Corrosion Inhibitors for Mild Steel in Acidic Environments. *RSC Adv.* **2015**, *5*, 11145−11162.
(62) Oguzie, E. E.; Enenebeaku, C. K.; Akalezi, C. O.; Okoro, S. C.; Ayuk, A. A.; Ejike, E. N. Adsorption and Corrosion-Inhibiting Effect of *Dacryodis edulis* Extract on Low-Carbon-Steel Corrosion in Acidic Media. *J. Colloid Interface Sci.* **2010**, *349*, 283−292.
(63) Casewit, C.; Colwell, K.; Rappe, A. Application of a Universal Force Field to Main Group Compounds. *J. Am. Chem. Soc.* **1992**, *114*, 10046−10053.
(64) Arab, S. T. Inhibition Action of Thiosemicabazone and Some of its *P*-Substituted Compounds on the Corrosion of Iron-Base Metallic Glass Alloy in 0.5 M H_2SO_4 at 30 °C. *Mater. Res. Bull.* **2008**, *43*, 510−521.
(65) Popova, A.; Christov, M.; Deligeorigiev, T. Influence of the Molecular Structure on the Inhibitor Properties of Benzimidazole Derivatives on Mild Steel Corrosion in 1 M Hydrochloric Acid. *Corrosion* **2003**, *59*, 756−764.
(66) Saha Kr, S.; Hens, A.; RoyChowdhury, A.; Lohar Kr, A.; Murmu, N. C.; Banerjee, P. Molecular Dynamics and Density Functional Theory Study on Corrosion Inhibitory Action of Three Substituted Pyrazine Derivatives on Steel Surface. *Canad. Chem. Trans.* **2014**, *2*, 489−503.
(67) Raczyńska, E. D.; Wozniak, K.; Dolecka, E.; Darowska, M. Superbasic Properties of the S═N Functional Group. *J. Phys. Org. Chem.* **2002**, *15*, 706−711.
(68) Makowski, M.; Raczyńska, E. D.; Chmurzyński, L. Ab Initio Study of Possible and Preferred Basic Site(s) in Polyfunctional N^1,N^1-Dimethyl-N^2-cyanoformamidine. *J. Phys. Chem. A* **2001**, *105*, 869−874.
(69) Raczyńska, E. D.; Darowska, M.; Dąbkowska, I.; Decouzon, M.; Gal, J. F.; Maria, P. C.; Poliart, C. D. Experimental and Theoretical Evidence of Basic Site Preference in Polyfunctional Superbasic Amidinazine: N^1,N^1-Dimethyl-N^2-β-(2-pyridylethyl)formamidine. *J. Org. Chem.* **2004**, *69*, 4023−4030.
(70) Raczyńska, D. E.; Makowski, M.; Górnicka, E.; Darowska, M. Ab Initio Studies on the Preferred Site of Protonation in Cytisine in the Gas Phase and Water. *Int. J. Mol. Sci.* **2005**, *6*, 143−156.
(71) Kumar, A. M.; Babu, R. S.; Obot, I. B.; Gasem, Z. M. Fabrication of Nitrogen Doped Graphene Oxide Coatings: Experimental and Theoretical Approach for Surface Protection. *RSC Adv.* **2015**, *5*, 19264−19272.
(72) Madhankumar, A.; Thangavel, E.; Ramakrishna, S.; Obot, I. B. Multi-functional Ceramic Hybrid Coatings on Biodegradable AZ31 Mg Implants: Electrochemical, Tribological and Quantum Chemical Aspects for Orthopaedic Applications. *RSC Adv.* **2014**, *4*, 24272−24285.
(73) Wade Jr. L. G. *Organic Chemistry*, 6th ed., Pearson Prentice Hall: Upper Saddle River, NJ, 2006.

DOI: 10.1021/acs.jpcc.5b03285
J. Phys. Chem. C 2015, 119, 16004−16019